Supporting Information

N-doped layered porous carbon electrodes with high mass loadings for high-performance supercapacitors

*Lizhi Sheng[1,] *, Yunyun Zhao[1], Baoquan Hou[2], Zhenpeng Xiao[1], Lili Jiang[2], and Zhuangjun Fan[3,] **

([1]Wood Material Science and Engineering Key Laboratory of Jilin Province, Beihua University, Jilin City 132013, PR China;

[2]Key Laboratory for Special Functional Materials in Jilin Provincial Universities, Jilin Institute of Chemical Technology, Jilin City 132022, PR China;

[3]School of Materials Science and Engineering, China University of Petroleum, Qingdao 266580, PR China)

*Corresponding author: E-mail: shengli_zhi@126.com (L. Sheng)

E-mail: fanzhj666@163.com (Z. Fan)

Electrochemical measurements:

The working electrodes were prepared by mixing obtained sample powders, super P and polytetrafluoroethylene (PTFE) with a mass ratio of 75:20:5 in ethanol to form a homogeneous slurry. Then the slurry was coated onto the nickel current collector (with a size of around 1 cm ×1 cm), and finally dried at 100 ℃ for 12 h in a vacuum oven. The mass loadings of active materials in various electrodes were ~1.0, 4.2, 7.8, 12.3 and 17.7 mg·cm^{-2},

respectively. In a three-electrode system, the as-prepared work electrode was clamped by a platinum electrode clip, with platinum foil as a counter electrode and Hg/HgO as a reference electrode. The cyclic voltammetry (CV), the galvanostatic charge-discharge (GCD) and the electrochemical impedance spectroscopy (EIS) tests were carried out in a 6 M KOH aqueous solution. The EIS measurements were evaluated in the frequency range from 100 kHz to 0.01 Hz at open circuit potential. The symmetric supercapacitors were assembled 1 M Na_2SO_4 aqueous solution using two identical work electrodes. The electrochemical measurements of symmetric supercapacitor were performed in a voltage window of 1.6 V, with 1 M Na_2SO_4 aqueous solution.

The specific capacitance (C_G, F g^{-1}) of the electrode material was calculated from GCD discharge curve:

$$C_G = \frac{I\Delta t}{m\Delta V} \tag{1}$$

Where I (A), Δt (s), ΔV (V), and m (g) are the constant discharge current, the discharge time, the discharge voltage, and the mass of the active material in the working electrode, respectively.

The areal specific capacitances based on the specific surface area (C_{SSA}, μF cm^{-2}) or geometric area of electrode (C_S, F cm^{-2}) were calculated as follow:

$$C_{SSA} = 100 \times C_G / A_{SSA} \tag{2}$$

$$C_A = C_G A_m \tag{3}$$

Where A_{SSA} (m^2 g^{-1}) and A_m (g cm^{-2}) are the specific surface area and mass loading of active materials.

The complex form of capacitance *C(w)* is dependent on real part the cell capacitance *C'(w)*, the imaginary part *C''(w)* related to the losses of energy dissipation and frequency, which is defined as follows:

$$C = C'(w) - jC''(w) \tag{4}$$

$$C'(w) = \frac{-Z''(w)}{w\left|Z(w)\right|^2} \tag{5}$$

$$C''(w) = \frac{Z'(w)}{w\left|Z(w)\right|^2} \tag{6}$$

Where *Z'*(*w*) and *Z''*(*w*) are the respective real and imaginary parts of the complex impedance *Z*(*w*). *w* is the angular frequency which is given by $w=2\pi f$.

The energy density (*E*, Wh kg^{-1}) and power density (*P*, W kg^{-1}) of the symmetric supercapacitor were calculated based on the following equations:

$$E = 0.5C\Delta V^2 / 3.6 \tag{7}$$

$$P = \frac{E}{\Delta t} \tag{8}$$

Where C is the specific capacitance based on the total mass or geometric area of active materials in two-electrode system. ΔV (V) and Δt (h) are the voltage after the Ohmic drop and the discharge time of the cell, respectively.

Fig. S1 photograph of metaplexis japonica shell.

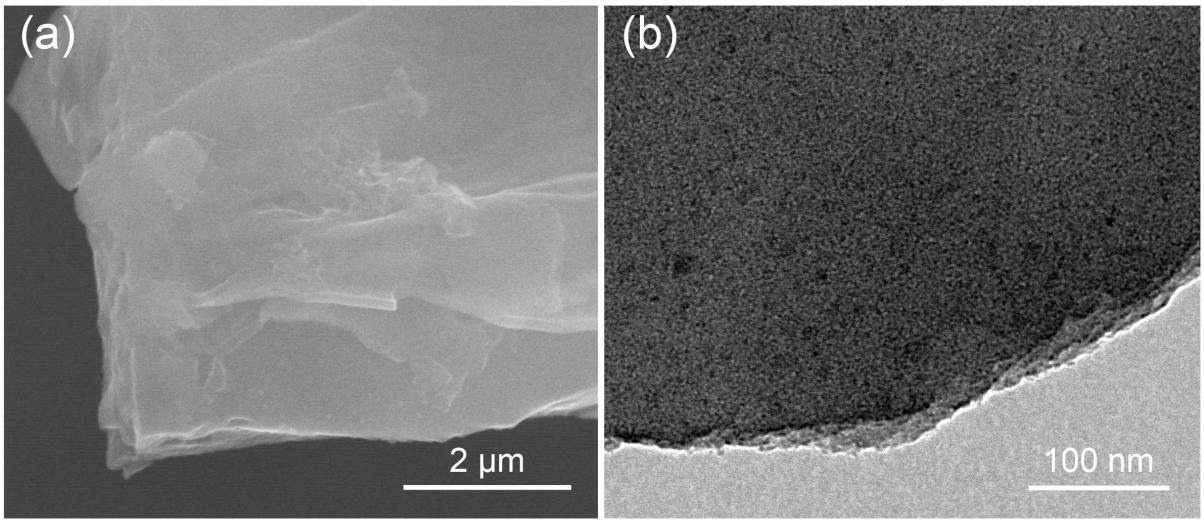

Fig. S2 (a) SEM and (b) TEM images of CM

Table S1 Pore structure parameters of CM, PCM and NPCM samples.

Sample	S_{BET} [$m^2\ g^{-1}$]	V_T [$cm^3\ g^{-1}$]	$V_{micro.}$ [$cm^3\ g^{-1}$]	$V_{meso.}$ [$cm^3\ g^{-1}$]
CM	50.6	0.042	0.038	0.004
PCM	317.0	0.190	0.163	0.027
NPCM	956.3	0.876	0.845	0.031

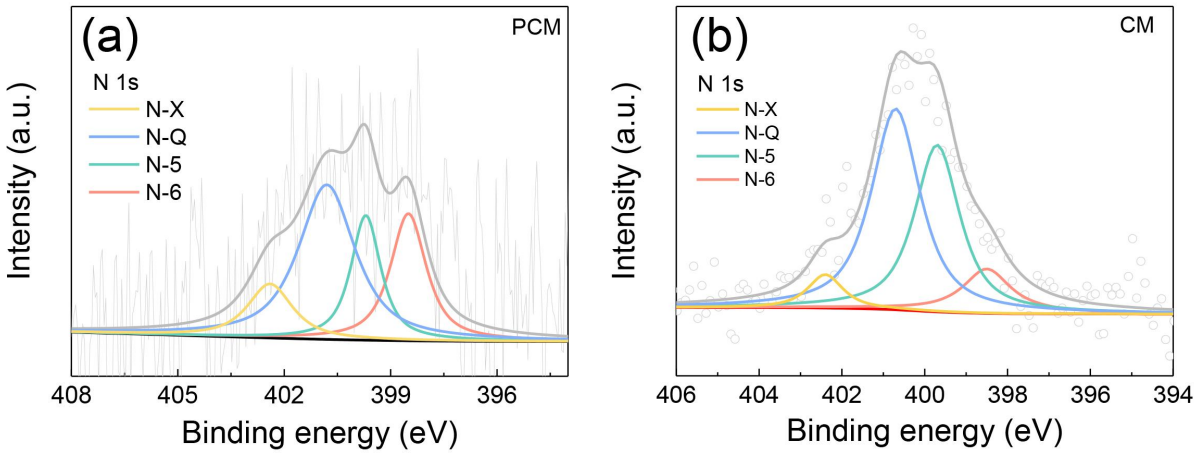

Fig. S3 High-resolution N 1s XPS spectrum of (a) PCM and (b) CM. Note: N-X, N-Q, N-5, N-6 denote oxidic, graphitic, pyrrolic, and pyridinic, respectively.

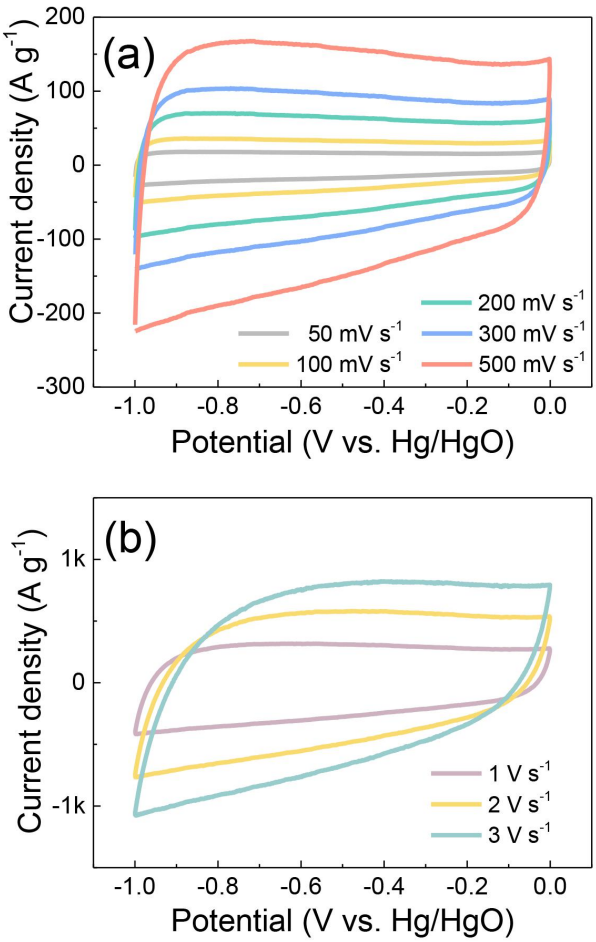

Fig. S4 CV curves of NPCM at various scan rates.

Table S2 Comparison of the specific capacitance and specific surface area of NPCM electrode with other biomass-derived heteroatom-doped carbon materials.

Materials	**C_g ($F\ g^{-1}$)**	**S_{BET} ($m^2\ g^{-1}$)**	**C_a ($\mu F\ cm^{-2}$)**	**Heteroatom**	**Ref.**
Hierarchical porous hollow-activated carbons	350 at 0.2 A g^{-1}	1641	21.3	N, O	[1]
Nitrogen-doped high-surface-area porous carbon	335 at 1 A g^{-1}	1751	19.1	N	[2]
Graphene-like porous carbon nanosheets	294 at 1 A g^{-1}	1051	28.0	N, S	[3]
Nitrogen-doped porous carbon nanosheets	324 at 0.05 A g^{-1}	2093	15.5	N	[4]
Heteroatom-doped sheet-like and hierarchical porous carbon	406 at 0.2 A g^{-1}	1535	26.4	N, O	[5]
N-O-S co-doped hierarchical porous carbons	301 at 0.5 A g^{-1}	1307	23.0	N, O, S	[6]
N/S-doped porous carbon	132 at 1 A g^{-1}	1575	8.4	N, S	[7]
Flexible 3D interconnected carbon	357 at 0.1 A g^{-1}	1456.4	24.5	B, N, O	[8]
N/S co-doped carbon material	222 at 1 A g^{-1}	1122.6	19.8	N, S	[9]
Nitrogen-graphitic hierarchical porous nanosheets	237 at 0.5 A g^{-1}	818.6	28.9	N	[10]
Dual-doped carbon frameworks	435 at 0.5 A g^{-1}	2000	21.8	N, O	[11]
O-N-S co-doped hierarchical porous carbons	576 at 1 A g^{-1}	2650	21.7	O, N, S	[12]
N, S co-doped carbon	317 at 1 A g^{-1}	2206	14.4	N, S	[13]
P/N co-doped porous carbon	568 at 1 A g^{-1}	2675	21.2	N, P	[14]
Activated porous carbon	317 at 1 A g^{-1}	1247.6	25.4	N, P	[15]
N-porous carbon	345 at 0.2 A g^{-1}	905.9	38.1	N	[16]
N-porous carbon	318 at 0.2 A g^{-1}	3006	10.6	N	[17]
Active carbon	328 at 1 A g^{-1}	2690	12.2	O, N, S	[18]
NPCM	**457 at 2 A g^{-1}**	**956.3**	**47.8**	**N**	**This work**

Table S3 Comparison of the specific capacitances and specific surface area of NPCM electrode with other biomass-derived activated carbon materials.

Materials	**C_g ($F\ g^{-1}$)**	**S_{BET} ($m^2\ g^{-1}$)**	**C_a ($\mu F\ cm^{-2}$)**	**Ref.**
Porous carbon	143 at 0.2 A g^{-1}	389	36.8	[19]
Three-dimensional carbon nanosheets	508 at 1 A g^{-1}	1612	31.5	[20]
Activated carbon	245 at 0.1 A g^{-1}	1958	12.5	[21]
Hierarchical porous carbon nanosheets	300 at 0.1 A g^{-1}	2687	11.2	[22]
Graphene-like porous active carbon	340 at 0.5 A g^{-1}	1015	33.5	[23]
Porous carbon nanosheets	350 at 0.1 A g^{-1}	1612	21.7	[24]
Porous carbon	413 at 1 A g^{-1}	3151	13.1	[25]
Porous carbon	427 at 0.5 A g^{-1}	2818	15.2	[26]
Activated carbon	294 at 1 A g^{-1}	2560	11.5	[27]
Activated carbon	247 at 1 A g^{-1}	1427.8	17.3	[28]
Activated carbon fiber	415 at 0.5 A g^{-1}	2289	18.1	[29]
Porous carbon	390 at 1 A g^{-1}	2131	18.3	[30]
Active carbon	167 at 1 A g^{-1}	911.92	18.3	[31]
Active carbon	161 at 0.2 A g^{-1}	682	23.6	[32]
Active carbon	406 at 0.5 A g^{-1}	2757.6	14.7	[33]
Active carbon	550 at 0.2 A g^{-1}	1265	43.5	[34]
Active carbon	254 at 0.5 A g^{-1}	2208	11.5	[35]
Active carbon	359 at 0.5 A g^{-1}	3089	11.6	[36]
Active carbon	285 at 0.5 A g^{-1}	1243.8	22.9	[37]
NPCM	**457 at 2 A g^{-1}**	**956.3**	**47.8**	**This work**

Table S4 EIS fitting results.

Sample	R_s (mΩ)	R_{ct} (mΩ)	C_{dl} (mF)	W_O-R	W_O-T	W_O-P
CM	83	120	2.27	0.08	0.055	0.448
PCM	58	50	3.53	0.174	0.031	0.484
NPCM	57	11	6.35	0.07	0.018	0.475

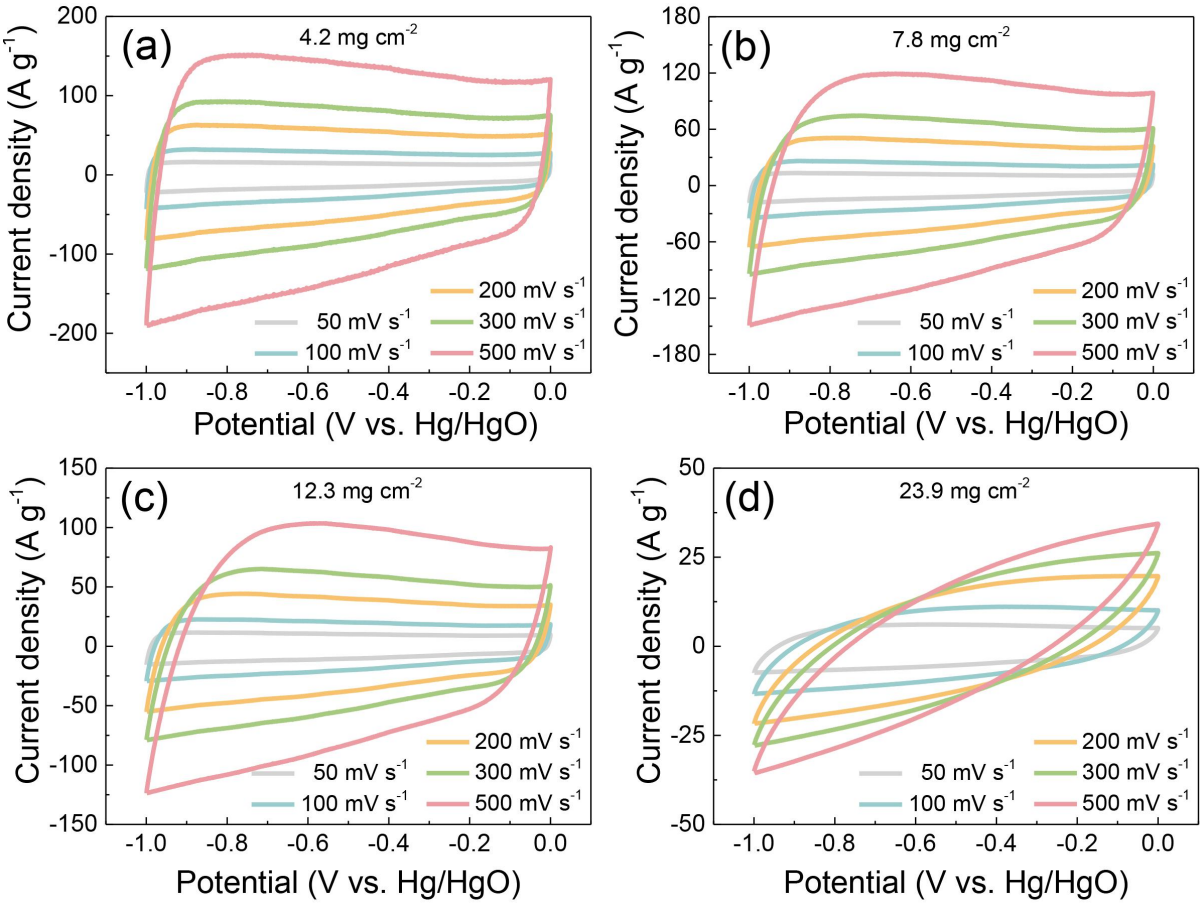

Fig. S5 CV curves of NPCM with various mass loading of (a) 4.2, (b) 7.8, (c) 12.3, and (d) 23.9 mg cm^{-2}, respectively.

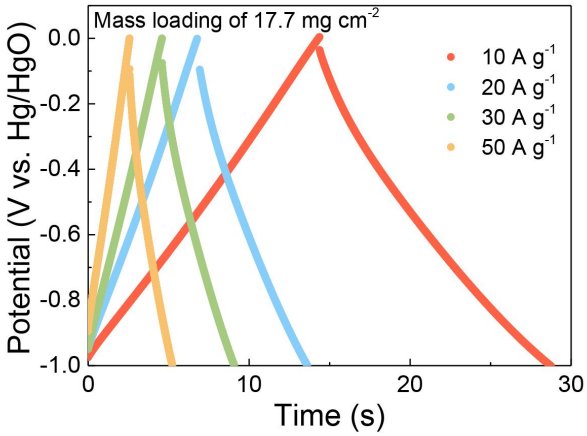

Fig. S6 GCD curves of NPCM at mass loading of 17.7 mg cm^{-2}.

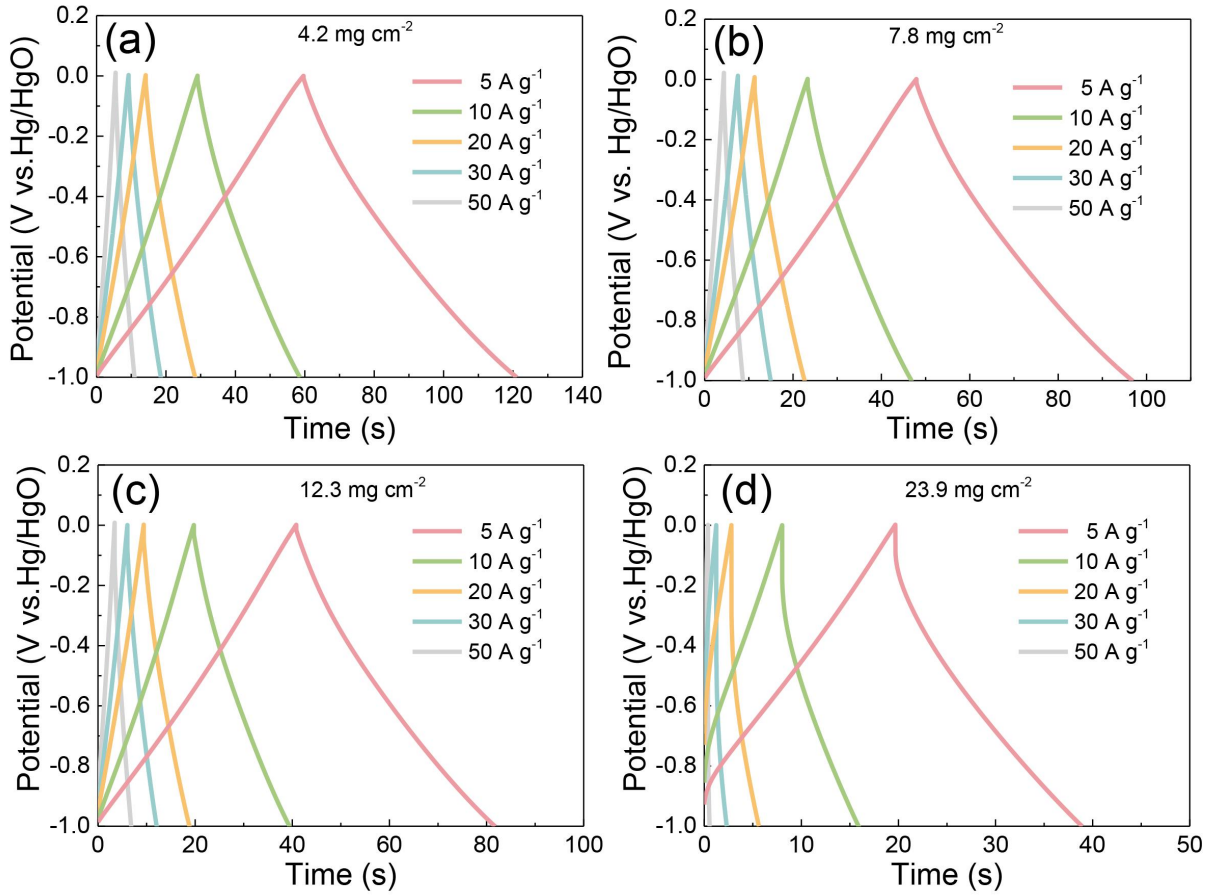

Fig. S7 GCD curves of NPCM with various mass loading of (a) 4.2, (b) 7.8, (c) 12.3, and (d) 23.9 mg cm^{-2}, respectively.

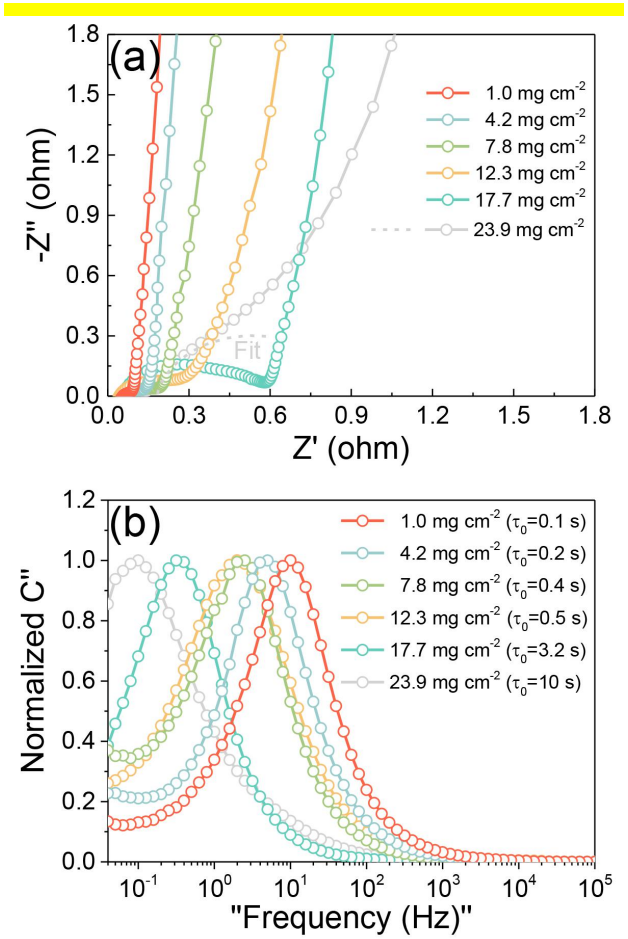

Fig. S8 (a) Nyquist plots and (b) Frequency response of the normalized capacitance of NPCM with different mass loading of 1.0, 4.2, 7.8, 12.3, 17.7 and 23.9 mg cm^{-2}.

.

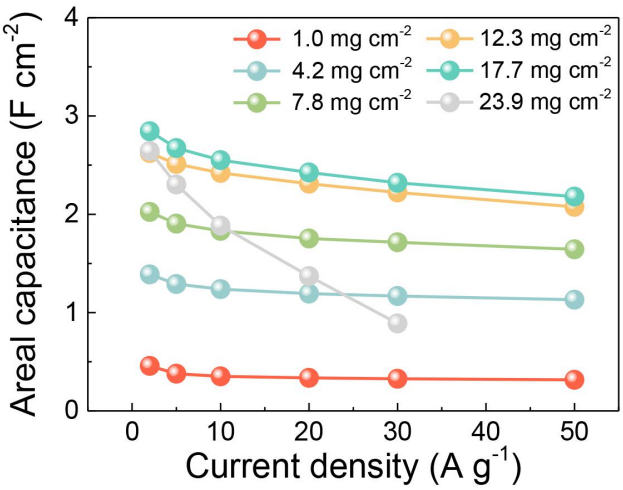

Fig. S9 Areal capacitance (based on the geometric area of electrode) of the NPCM electrodes with different mass loadings.

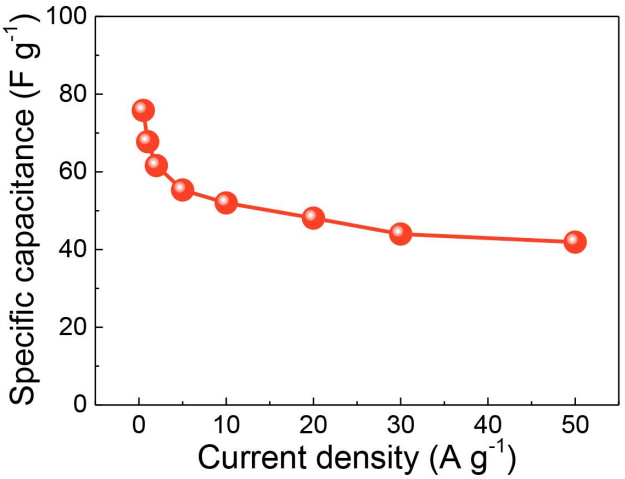

Fig. S10 Gravimetric capacitance of the NPCM//NPCM at different current density.

References

[1] Yan R, Wang K, Tian X, et al. Heteroatoms in situ-doped hierarchical porous hollow-activated carbons for high-performance supercapacitor [J]. Carbon Letters, 2019, 30 (3): 331–344.

[2] Zhou J, Wang M, Li X. Facile preparation of nitrogen-doped high-surface-area porous carbon derived from sucrose for high performance supercapacitors [J]. Applied Surface Science, 2018, 462: 444–452.

[3] Liu B, Yang M, Chen H, et al. Graphene-like porous carbon nanosheets derived from

salvia splendens for high-rate performance supercapacitors [J]. Journal of Power Sources, 2018, 397: 1–10.

[4] Guan L, Pan L, Peng T, et al. Synthesis of biomass-derived nitrogen-doped porous carbon nanosheests for high-performance supercapacitors [J]. ACS Sustainable Chemistry & Engineering, 2019, 7 (9): 8405–8412.

[5] Lin Y, Chen Z, Yu C, et al. Heteroatom-doped sheet-like and hierarchical porous carbon based on natural biomass small molecule peach gum for high-performance supercapacitors [J]. ACS Sustainable Chemistry & Engineering, 2019, 7 (3): 3389–3403.

[6] Liu F, Wang Z, Zhang H, et al. Nitrogen, oxygen and sulfur co-doped hierarchical porous carbons toward high-performance supercapacitors by direct pyrolysis of kraft lignin [J]. Carbon, 2019, 149: 105–116.

[7] Chen Y, Hu R, Qi J, et al. Sustainable synthesis of N/S-doped porous carbon sheets derived from waste newspaper for high-performance asymmetric supercapacitor [J]. Materials Research Express, 2019, 6 (9): 095605.

[8] Dai P, Xue Y, Zhang S, et al. Paper-derived flexible 3D interconnected carbon microfiber networks with controllable pore sizes for supercapacitors [J]. ACS Applied Materials & Interfaces, 2018, 10 (43): 37046–37056.

[9] Zhao N, Zhang P, Luo D, et al. Direct production of porous carbon nanosheets/particle composites from wasted litchi shell for supercapacitors [J]. Journal of Alloys and Compounds, 2019, 788: 677–684.

[10] Li P, Xie H, Liu Y, et al. Molten salt and air induced nitrogen-containing graphitic hierarchical porous biocarbon nanosheets derived from kitchen waste hydrolysis residue for energy storage [J]. Journal of Power Sources, 2019, 439: 227096.

[11] Li Z, Mi H, Bai Z, et al. Sustainable biowaste strategy to fabricate dual-doped carbon frameworks with remarkable performance for flexible solid-state supercapacitors [J]. Journal of Power Sources, 2019, 418: 112–121.

[12] Zhao G, Chen C, Yu D, et al. One-step production of O-N-S co-doped three-dimensional hierarchical porous carbons for high-performance supercapacitors [J]. Nano Energy, 2018, 47: 547–555.

[13] Wang B, Ji L, Yu Y, et al. A simple and universal method for preparing N, S co-doped

biomass derived carbon with superior performance in supercapacitors [J]. Electrochimica Acta, 2019, 309: 34–43.

[14] Wang N, Wang C, He L, et al. Incomplete phase separation strategy to synthesize P/N co-doped porous carbon with interconnected structure for asymmetric supercapacitors with ultra-high power density [J]. Electrochimica Acta, 2019, 298: 717–725.

[15] Wang Y, Zhang M, Dai Y, et al. Nitrogen and phosphorus co-doped silkworm-cocoon-based self-activated porous carbon for high performance supercapacitors [J]. Journal of Power Sources, 2019, 438: 227045.

[16] Yu S, Zhu X, Lou G, et al. Sustainable hierarchical porous biomass carbons enriched with pyridinic and pyrrolic nitrogen for asymmetric supercapacitor [J]. Materials & Design, 2018, 149: 184–193.

[17] Xu D, Su Y, Zhang S, et al. Highly porous N-doped carbons production from biomass for high-performance supercapacitors without chemical nitrogen-containing dopants [J]. Energy Sources, Part A: Recovery, Utilization, and Environmental Effects, 2019, 42 (14): 1797–1807.

[18] Guo N, Luo W, Guo R, et al. Interconnected and hierarchical porous carbon derived from soybean root for ultrahigh rate supercapacitors [J]. Journal of Alloys and Compounds, 2020, 834: 155115.

[19] Gopalakrishnan A, Badhulika S. Ultrathin graphene-like 2D porous carbon nanosheets and its excellent capacitance retention for supercapacitor [J]. Journal of Industrial and Engineering Chemistry, 2018, 68: 257–266.

[20] Liu M, Zhang K, Si M, et al. Three-dimensional carbon nanosheets derived from micro-morphologically regulated biomass for ultrahigh-performance supercapacitors [J]. Carbon, 2019, 153: 707–716.

[21] Cao Y, Wang X, Gu Z, et al. Potassium chloride templated carbon preparation for supercapacitor [J]. Journal of Power Sources, 2018, 384: 360–366.

[22] Yao Y, Xiao Z, Liu P, et al. Facile synthesis of 2D ultrathin and ultrahigh specific surface hierarchical porous carbon nanosheets for advanced energy storage [J]. Carbon, 2019, 155: 674–685.

[23] Lu S-Y, Jin M, Zhang Y, et al. Chemically exfoliating biomass into a graphene-like

porous active carbon with rational pore structure, good conductivity, and large surface area for high-performance supercapacitors [J]. Advanced Energy Materials, 2018, 8 (11): 1702545.

[24] Yu D, Chen C, Zhao G, et al. Biowaste-derived hierarchical porous carbon nanosheets for ultrahigh power density supercapacitors [J]. ChemSusChem, 2018, 11 (10): 1678–1685.

[25] Yu P, Liang Y, Dong H, et al. Rational synthesis of highly porous carbon from waste bagasse for advanced supercapacitor application [J]. ACS Sustainable Chemistry & Engineering, 2018, 6 (11): 15325–15332.

[26] Zhang Q, Han K, Li S, et al. Synthesis of garlic skin-derived 3D hierarchical porous carbon for high-performance supercapacitors [J]. Nanoscale, 2018, 10 (5): 2427–2437.

[27] Du W, Zhang Z, Du L, et al. Designing synthesis of porous biomass carbon from wheat straw and the functionalizing application in flexible, all-solid-state supercapacitors [J]. Journal of Alloys and Compounds, 2019, 797: 1031–1040.

[28] Guo F, Jiang X, Jia X, et al. Synthesis of biomass carbon electrode materials by bimetallic activation for the application in supercapacitors [J]. Journal of Electroanalytical Chemistry, 2019, 844: 105–115.

[29] Li M, Xiao H, Zhang T, et al. Activated carbon fiber derived from sisal with large specific surface area for high-performance supercapacitors [J]. ACS Sustainable Chemistry & Engineering, 2019, 7 (5): 4716–4723.

[30] Song M, Zhou Y, Ren X, et al. Biowaste-based porous carbon for supercapacitor: The influence of preparation processes on structure and performance [J]. Journal of Colloid and Interface Science, 2019, 535: 276–286.

[31] Song X, Ma X, Li Y, et al. Tea waste derived microporous active carbon with enhanced double-layer supercapacitor behaviors [J]. Applied Surface Science, 2019, 487: 189–197.

[32] Wang Y, Ding B, Guo D, et al. A novel way to synthesize nitrogen and oxygen co-doped porous carbon for high performance supercapacitors [J]. Microporous and Mesoporous Materials, 2019, 282: 114–120.

[33] Wu F, Gao J, Zhai X, et al. Hierarchical porous carbon microrods derived from albizia flowers for high performance supercapacitors [J]. Carbon, 2019, 147: 242–251.

[34] Yang S, Wang S, Liu X, et al. Biomass derived interconnected hierarchical

micro-meso-macro-porous carbon with ultrahigh capacitance for supercapacitors [J]. Carbon, 2019, 147: 540–549.

[35] He J, Zhang D, Wang Y, et al. Biomass-derived porous carbons with tailored graphitization degree and pore size distribution for supercapacitors with ultra-high rate capability [J]. Applied Surface Science, 2020, 515: 146020.

[36] Liu Y, Qu X, Huang G, et al. 3-dimensional porous carbon with high nitrogen content obtained from longan shell and its excellent performance for aqueous and all-solid-state supercapacitors [J]. Nanomaterials, 2020, 10 (4): 808.

[37] Xu L, Li X, Li X Large-sized and ultrathin biomass-derived hierarchically porous carbon nanosheets prepared by a facile way for high-performance supercapacitors [J]. Applied Surface Science, 2020, 526: 146770.